Electrostatic interaction between SARS-CoV-2 and charged surfaces: Spike protein evolution changed the game

Marc Domingo,[†] Horacio V. Guzman,[‡] Matej Kanduč,[¶] and Jordi Faraudo[*,†]

[†]*Institut de Ciència de Materials de Barcelona (ICMAB-CSIC), Campus de la UAB, E-08193 Bellaterra, Spain*

[‡]*Departamento de Física Teórica de la Materia Condensada, Universidad Autónoma de Madrid, Spain*

[¶]*Department of Theoretical Physics, Jožef Stefan Institute, Ljubljana, Slovenia.*

E-mail: jfaraudo@icmab.es

Abstract

Previous works show a key role of electrostatics for the SARS-CoV-2 virus in aspects such as virus-cell interactions or virus inactivation by ionic surfactants. Electrostatic interactions depend strongly on the variant since the charge of the Spike protein (responsible for virus - environment interactions) evolved across the variants from the highly negative Wild Type (WT) to the highly positive Omicron variant. The distribution of the charge also evolved from diffuse to highly localized. These facts suggest that SARS-CoV-2 should interact strongly with charged surfaces in a way that changed during the virus evolution.

This question is studied here by computing the electrostatic interaction between WT, Delta and Omicron Spike proteins with charged surfaces using a new method (based on Debye-Hückel theory) that provides efficiently general results as a function of the surface charge density σ. We found that the interaction of the WT and Delta variant spikes with charged surfaces is dominated by repulsive image forces proportional to σ^2 originated at the protein/water interface. On the contrary, the Omicron variant shows a distinct behaviour, being strongly attracted to negatively charged surfaces and repelled from positively charged ones. Therefore, the SARS-CoV-2 virus has evolved from being repelled by charged surfaces to being efficiently adsorbing to negatively charged ones.

1 Introduction

From the physico-chemical point of view, viruses can be considered as colloidal particles, and, for this reason, there is a long tradition in the use of concepts and theories of colloidal forces to understand how viruses interact with the environment.[1] Classical DLVO (Derjaguin-Landau-Verwey-Overbeek) theory and its extensions have been widely applied to viruses, to study questions such as virus adsorption, filtration and removal from environment[2–4] or virus stability and aggregation.[5] AFM force measurements over viruses are also interpreted in the framework of DLVO theory.[6,7] The Poisson-Boltzmann equation describing electrostatics in salt solution (a key ingredient of the classical theory of colloidal forces) can be solved numerically with high resolution,[8] so it is possible to obtain a detailed tomography of electrostatic forces over virus capsids.[7] These calculations are obviously difficult, but new developments allow accurate and efficient numerical calculations of electrostatic forces between atomistic models of large supramolecular structures such as viruses and other charged objects or surfaces.[9]

It should be noted that the vast majority of the studies mentioned above deal with naked viruses based on protein capsids (non-enveloped viruses), whereas many relevant viruses (like those related to respiratory illnesses such as coronaviruses and flu viruses) are enveloped viruses,[10,11] in which the inner structure of the virus is covered by a lipid envelope decorated with large glycoproteins that protrude towards the environment. This fact justifies that, as the COVID-19 pandemic arrived, many studies were developed trying to identify which physico-chemical interactions were relevant for the new SARS-CoV-2 enveloped virus.[12,13] One of the most promising approaches was the use of AFM force microscopy to accurately measure the forces between the virus and different materials.[14,15] In these studies, the AFM tip was covered with SARS-CoV-2 Spike proteins, which is the glycoprotein that protrudes from the virus envelope, responsible for its infectivity and its interaction with the environment. The Spike of SARS-CoV-2 is strongly charged, so in principle, strong electrostatic interactions can be expected.[16] However, these studies[14,15] were not able to identify relevant

electrostatic interactions between the Spike protein and surfaces of materials.

Explicit examples of important electrostatic effects for SARS-CoV-2 were identified by subsequent work. One key example of the importance of electrostatic effects was provided by experimental studies on the mechanism of inactivation of coronaviruses by surfactants,[17] which were motivated by predictions based on earlier Molecular Dynamics (MD) multi-scaling simulations.[18] It was shown that ionic surfactants are much more efficient against coronaviruses than non-ionic ones due to their ability to block and eventually denaturalize their spike proteins. In fact, anionic surfactants were the most efficient ones.[17,18] The reason is that, as predicted by MD simulations, ionic surfactants inactivate the virus by collapsing the Spike protein, instead of compromising the virus envelope integrity. Anionic surfactants are the most effective because they easily block the receptor binding domain (RBD) by interacting with positively charged amino acids and hydrophobic side chains. This preference of binding to anionic surfactants compared to cationic ones was unexpected since the Wild Type spike protein considered there has an overall negative charge. This is an interesting observation that demonstrates the importance of considering the local electrostatic environment instead of the total charge only.

The amount of positive charge in the Spike protein, and in particular, in the residues at and around the RBD, has increased during the evolution of the different variants of the virus.[19–21] The variant with the largest positive charge around the RBD is the Omicron variant, which is substantially more infectious than previous variants. Electrostatic interactions play a decisive role in the binding of the Spike protein to the ACE2 cellular receptor[19] as well as in key intermediate steps of the infection process such as the binding of the virus to the cellular glycocalyx.[21,22] This binding occurs through electrostatic interactions between the Spike of the virus and the heparan sulfate of the cellular glycocalyx, which has a large and homogeneous negative charge density.[21,22] The charged residues at the Spike protein region involved in this interaction are different for each virus variant, being more positive for the Omicron variant and therefore leading to a stronger interaction with heparan sulfate, as

demonstrated by Poisson-Boltzmann calculations.[21] This result not only explains the larger infectivity of the Omicron variant but also can be used to design improved diagnosing strips for each variant.[21]

Electrostatic interactions are also present in many other aspects of SARS-CoV-2. For example, electrostatics plays a role in the capture of SARS-CoV-2 by masks and filters, which in some cases have charged electret fibres.[23] Poisson-Boltzmann calculations also provided the energetic differences between conformations of the SARS-CoV-2 Spike Protein.[24]

These previous results motivate the interest of a more generic study of the electrostatic interaction between different variants of the SARS-CoV-2 virus and charged surfaces. Since there are many situations involving the interaction between a virus and a solid/liquid interface (e.g., fomite contamination, virus capture, transport and spreading of viruses adsorbed over particles) it is relevant to understand how the charge of these surfaces impacts the interaction with the different variants of the virus (which have different charges and different charge distributions).

In our previous studies, we focused our efforts on developing detailed atomistic simulations of the interaction of the SARS-CoV-2 virus with specific materials.[13,25–28] In contrast, our aim here is to obtain general results to understand how generic surfaces, described by global properties such as charge density and dielectric constant impact the interaction with the different variants of the SARS-CoV-2 virus.

To this end, we will simplify the SARS-CoV-2 virus-surface interaction by considering the electrostatic interaction of the different Spike protein variants (Wild Type, Delta and Omicron) with charged surfaces, as shown schematically in Figure 1. We will employ the Poisson-Boltzmann theory in its linear approximation (Debye-Hückel theory), which provided good results for the different variants in Ref.[21] The Spike proteins will be described atomistically (using structures obtained in previous works), whereas the models of the surfaces will be generic.

In order to explore systematically these interactions for different charge densities, we in-

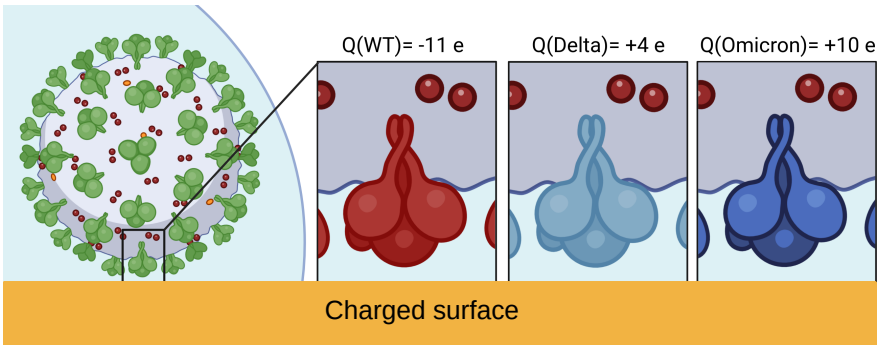

Figure 1: Scheme of the interaction between a SARS-CoV-2 virus with a surface through its Spike proteins (the virion particle is considered to be inside a water droplet or in aqueous solvent). The charge of the spike protein is indicated for the Wild Type (WT) and the Delta and Omicron variants of concern. Figure created with BioRender.com

troduce here a method to efficiently compute the electrostatic interaction between a protein structure and charged surfaces at the linear Poisson-Boltzmann (PB) level. The method provides a general expression for the free energy of interaction between an atomistic model of a protein and a material with arbitrary surface charge, which depends on a few physically interpretable coefficients that are determined employing a reduced set of appropriately designed numerical PB calculations. Each coefficient encodes particular interactions such as image or direct charge-charge interactions, allowing us to dissect the different contributions to the calculated interactions. The method does not include further approximations beyond linear PB. The method is employed to study systematically how three different virus variants (WT, Delta and Omicron) interact with surfaces depending on their surface charge density.

We also analyze in detail the effect of environmental variables such as the salt concentration or modelling details such as the impact of considering different specific configurations of the same protein variant.

Using the methods developed here, we will show that the Omicron variant has a distinct behaviour, different from that of WT and Delta. The fact that the Omicron variant has a more homogeneous, well-defined charge distribution substantially enhances its electrostatic interactions, being attracted by negatively charged surfaces and repelled by positively charged ones. On the contrary, the more heterogeneous charge distribution in the Wild Type

and Delta spike proteins produces an inefficient (weak) direct electrostatic interaction with charged surfaces. In this case, the interaction with charged surfaces is mostly given by the image charge repulsion originated at the protein/water dielectric discontinuity.

2 Theory, Modelling and Numerical Methods

2.1 Formulation of the problem

The problem considered in our calculations is shown schematically in Figure 2. Given atomistic models for the Spike proteins of WT, Delta and Omicron variants of the SARS-CoV-2 virus, we would like to study their electrostatic interaction with a uniformly charged surface in a salty water environment.

The problem will be analyzed using the Debye-Hückel theory (Poisson - Boltzmann theory in the linear approximation). This is the same level of approximation considered in previous work that analyzed the different electrostatic interactions of WT, Delta and Omicron Spike proteins during the infection mechanism.[21]

The Spike protein is assumed to be in a perpendicular orientation to the surface, with the receptor binding domain exposed towards the surface (see Figure 2). As seen in the figure, the protein atoms closer to the surface are those from the RBD and from some labile glycans. In order to characterize the distance between the protein structure and the surface in this figure, we define the distance d_c between the surface and the closest protein atom as well as the distance $d_{\text{RBD-CM}}$ between the center of the receptor binding domain RBD and the surface.

It should be noted that the mobility of glycans and other labile residues may affect the electrostatic interaction between the protein and the surface. This will be taken into consideration by repeating the calculations for different characteristic protein configurations, as identified by molecular dynamics simulations (see subsection 2.3).

The main quantity of interest in our calculations is the free energy of interaction, G,

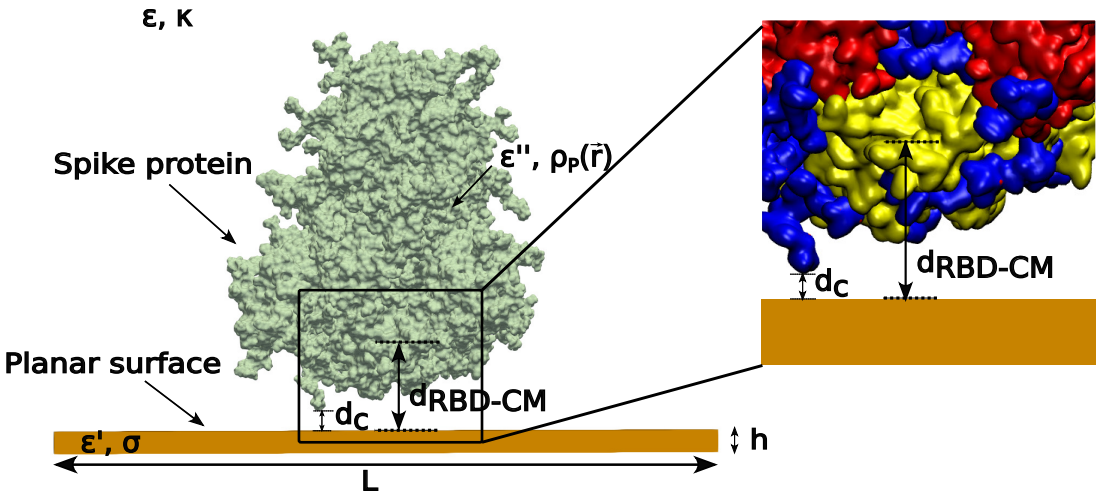

Figure 2: Scheme of the model considered in the Poisson-Boltzmann calculations for the interaction between a spike protein in salty water and a surface. The different quantities (dielectric constant, charge distribution) characterizing the protein, the solvent and the surface are also indicated. The inset highlights several relevant features of the spike protein. The receptor binding domain (RBD, residues 333 to 527) are indicated in yellow, glycans are shown in blue and the rest of the protein is shown in red. We also indicate the distance d_c between the surface and the closest protein atom and the distance d_{RBD-CM} between the center of the receptor binding domain RBD and the surface.

between the protein and the surface, as a function of their separation. The protein-surface separation will be indicated by d, which has to be understood as a generic label for the position of the protein relative to the surface (it can be d_c or $d_{\text{RBD-CM}}$ or another suitable measure of the protein location relative to the surface). In the Debye-Hückel theory, $G(d)$ can be computed by the following expression originally derived by Verwey and Overbeek:[29]

$$G(d) = \frac{1}{2}\int \rho(\vec{r})\phi(\vec{r};d)d\vec{r}, \tag{1}$$

where $\rho(\vec{r})$ is the charge distribution of the system and $\phi(\vec{r};d)$ is the electrostatic potential. The charge distribution includes the atomic charges from the protein structure ($\rho_p(\vec{r})$) and those from the planar surface with surface charge density σ located at $z = z_0$ (Figure 2):

$$\rho(\vec{r}) = \rho_p(\vec{r}) + \sigma\delta(z - z_0). \tag{2}$$

In the linear PB approximation, the electrostatic potential obeys:[29,30]

$$\begin{aligned} \nabla^2\phi &= \kappa^2\phi \text{ (inside electrolyte solution)} \\ \nabla^2\phi &= \frac{1}{\varepsilon_r^{in}}\rho(\vec{r}) \text{ (inside protein or material)} \end{aligned} \tag{3}$$

where $\kappa = 1/\lambda_{DH}$ is the inverse of the Debye length and ε_r^{in} is the dielectric constant inside the protein or the material. The boundary conditions at the water/protein and the water/surface interfaces are continuity of the dielectric displacement (ε_r^w is the dielectric constant of water):

$$\varepsilon_r^w \left.\frac{\partial\phi}{\partial n}\right|_w = \varepsilon_r^{in} \left.\frac{\partial\phi}{\partial n}\right|_{in} \text{ at interfaces} \tag{4}$$

and continuity of the potential across interfaces. The boundary condition given by Eq.(4) is responsible for the so-called image-charge forces that appear due to the dielectric discontinuity at interfaces (particularly at the water/protein interface, as we will see later).

Due to the complexity of the problem, the only way to obtain explicit results is by solving numerically Eqs. (2)-(4) to determine $\phi(\vec{r};d)$ and then integrate Eq.(1) numerically. This task will be performed using the PyGBe software,[8,30] which was specially designed for biomolecular electrostatics calculations. This program has been used previously in many biophysics problems such as the prediction of the orientation of proteins and antibodies onto sensors,[31,32] the study of disassembly of viral capsids[33] and the calculation of forces of viral capsids approaching a nanometric probe.[7]

2.2 General expression for the Electrostatic Free Energy

Before resorting to numerical calculations, we will derive here analytical expressions that simplify the analysis of the protein-surface interaction problem. Our derivation is based on the fact that the free energy $G(d)$ given by Eq.(1) can be written in the following alternative way:[34]

$$G(d) = \frac{1}{2}\iint \rho(\vec{r})u(\vec{r},\vec{r}\,';d)\rho(\vec{r}\,')d\vec{r}d\vec{r}\,', \tag{5}$$

where $u(\vec{r},\vec{r}';d)$ is the Green function associated with the linear PB equation including the boundary conditions at the dielectric discontinuities (i.e., the solution of Eqs.(3) and (4) with a point source unit charge at $\vec{r}'$). As the separation between the protein and the surface increases ($d \to \infty$), the Green function $u(\vec{r},\vec{r}';d)$ approaches the isotropic Green function $u_0(\vec{r},\vec{r}')$ for the linear PB equation in a pure electrolyte solution (in absence of any dielectric discontinuity) and the free energy $G(d)$ approaches the electrostatic self-energy G_0 of the individual components of the system (the protein and the surface).

We are interested in how the free energy varies with protein-surface separation, d, relative to that at infinite separation:

$$\Delta G(d) = G(d) - G_0 = \frac{1}{2}\iint \rho(\vec{r})u^*(\vec{r},\vec{r}';d)\rho(\vec{r}')d\vec{r}d\vec{r}', \tag{6}$$

where we have defined:

$$u^*(\vec{r},\vec{r}';d) = u(\vec{r},\vec{r}';d) - u_0(\vec{r},\vec{r}'). \tag{7}$$

The dependence of the free energy on the surface charge σ can be obtained analytically by substituting Eq.(2) into Eq.(6):

$$\begin{aligned}\Delta G(d) &= \frac{1}{2}\iint \rho_p(\vec{r})u^*(\vec{r},\vec{r}';d)\rho_p(\vec{r}')d\vec{r}d\vec{r}' \\ &+ \frac{\sigma}{2}\iint (\rho_p(\vec{r})u^*(\vec{r},\vec{r}';d)\delta(z'-z_0) + \delta(z-z_0)u^*(\vec{r},\vec{r}';d)\rho_p(\vec{r'}))d\vec{r}d\vec{r}' \\ &+ \frac{\sigma^2}{2}\iint \delta(z-z_0)u^*(\vec{r},\vec{r}';d)\delta(z'-z_0)d\vec{r}d\vec{r}'.\end{aligned} \tag{8}$$

Eq.(8) can be written in a more compact way by noting that we have three different contributions: one independent of σ, one proportional to σ and one proportional to σ^2, so we have:

$$\Delta G(d) = g_{\text{self\_prot}}(d) + g_\sigma(d)\sigma + g_{\text{self\_plane}}(d)\sigma^2. \tag{9}$$

The three coefficients $g_{\text{self\_prot}}(d)$, $g_\sigma(d)$ and $g_{\text{self\_plane}}(d)$ correspond to the three groups of integrals appearing in Eq.(8).

Eq.(9) shows that the protein-surface interaction has a simple analytical dependence on the surface charge density σ, which is a consequence of the Debye-Hückel theory (no further approximations are needed).

A close inspection of Eqs.(8) and (9) also provides a physical interpretation for the different contributions. The term easiest to interpret is the contribution $g_\sigma(d)$ (free energy term proportional to σ), which accounts for the interactions between protein charges and surface charges (both real and image charges). The other two terms account for interactions of charges with their own image charges, generated due to dielectric discontinuities. The first term (encoded by the $g_{\text{self\_prot}}(d)$) is independent of σ and accounts for the interaction of the protein charges with their image charges generated by the dielectric discontinuity at the solid-liquid interface. Analogously, the coefficient $g_{\text{self\_plane}}$ (contribution quadratic in σ) depends only on the charges from the surface, and it accounts for the interactions of the planar surface charges with their images generated by the dielectric discontinuity at the water/protein interface.

2.3 Method for the Calculation of the contributions to the Electrostatic Free Energy

A brute-force exploration of the effect of different surface charges in the protein-surface interaction requires the calculation of $\Delta G(d)$ for each considered value of σ, which is a tedious task involving a large number of calculations. However, there is no need of such a brute-force approach, since the results of the previous section (Eqs. (8) and (9)) allow the numerical calculation of the free energy as a function of σ from a reduced number of independent calculations, only three for a given d. The proposed calculations are shown schematically in Figure 3 and summarized in Table 1.

The first calculation to be performed in our method is the full calculation of $\Delta G(d)$ for a particular (arbitrary) value of the charge density numerically using Eqs.(1)-(4). This system will be denoted as the *reference system*, its charge density denoted as σ_{ref} and the resulting

Table 1: Parameters used in the three calculations required to determine the coefficients $g_{self\_prot}(d)$, $g_{\sigma}(d)$ and $g_{self\_plane}(d)$ in Eq.(9) following the method described in the text.

Simulated System	Protein charge	Surface charge	Result	Calculated coefficient
Auxiliary I	$\rho_p(\vec{r})$	0	$\Delta G_{\rm I}$	$g_{\rm self\_prot} = \Delta G_{\rm I}$
Auxiliary II	0	$\sigma_{\rm ref}$	$\Delta G_{\rm II}$	$g_{\rm self\_plane} = \Delta G_{\rm II}/\sigma^2_{\rm ref}$
Reference system	$\rho_p(\vec{r})$	$\sigma_{\rm ref}$	$\Delta G_{\rm ref}$	g_{σ} (Eq.12)

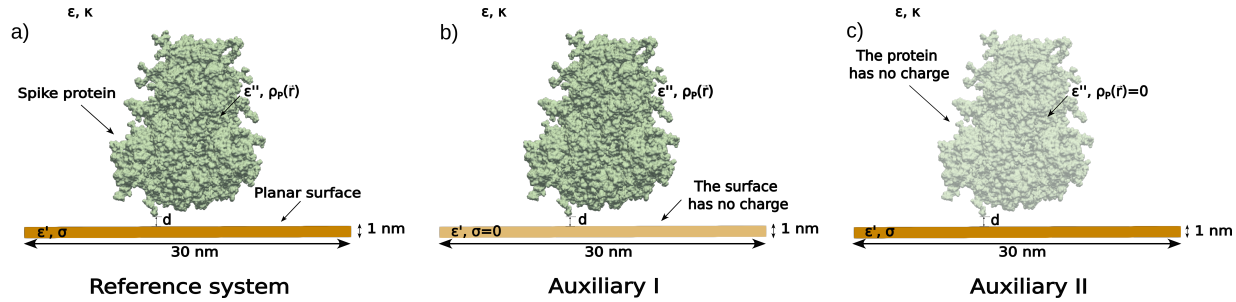

Figure 3: Scheme of the three calculations summarized in Table 1 needed for the calculation of the terms of the protein-surface interaction free energy given by Eq.(9). The protein or the surface are depicted as translucent when all its charges are set to zero. (a) The reference system, (b) Auxiliary system I and (c) Auxiliary system II.

free energy calculation denoted as $\Delta G_{\rm ref}$.

In addition, we consider two specially designed cases, which we denote as Auxiliary systems I and II (see Table 1 and Figure 3). Auxiliary system I corresponds to a particular solution of the linear PB problem (Eqs.(1)-(4)) with $\sigma = 0$. This solution captures the interaction between the protein charge and the dielectric discontinuity at the water-surface interface. The resulting free energy is denoted by $\Delta G_I(d)$.

Auxiliary system II corresponds to an analogous calculation but this time setting all partial charges of the protein to zero and the charge density of the material surface to σ_{ref} . The resulting free energy ($\Delta G_{II}(d)$) encodes how the charge of the surface plane interacts with the dielectric discontinuity at the water/protein interface. In each of these auxiliary calculations, only one of the integrals in Eq.(8) is different from zero, so these calculations directly provide two of the coefficients defined in Eq.(9):

$$g_{\rm self\_prot}(d) = \Delta G_{\rm I}(d). \tag{10}$$

$$g_{\text{self\_plane}}(d) = \frac{1}{\sigma_{\text{ref}}^2}\Delta G_{II}(d). \tag{11}$$

Now, the result for the reference system $\Delta G_{ref}(d)$ can be easily used to compute the remaining unknown term ($g_\sigma(d)$) by substituting Eqs. (10) and (11) in Eq. (9) and using $\sigma = \sigma_{\text{ref}}$:

$$g_\sigma(d) = \frac{1}{\sigma_{\text{ref}}}\left[\Delta G_{ref}(d) - \Delta G_I(d) - \Delta G_{II}(d)\right]. \tag{12}$$

In summary, the method requires performing three calculations summarized in Table 1. The results of the simulations are then used in Eqs.(10)-(12) to determine the three coefficients $g_{\text{self\_prot}}(d)$, $g_\sigma(d)$ and $g_{\text{self\_plane}}(d)$ of the free energy appearing in Eq.(9). In that way, we can obtain the results for any desired value of σ (Eq.(9)) without the need of repeating the calculations for each value of σ.

In the ESI, we provide a numerical verification of the validity of the method, including explicit examples showing that the results of Eqs.(11) and (12) are independent of the chosen value of σ_{ref}.

2.4 Numerical methods

Here we provide a brief description of the performed calculations (see full details in the Supporting Information).

All numerical results reported in this paper were obtained using the PyGBe sofware.[8,30] We should emphasize that the values employed for the parameters of the numerical calculations in PyGBe (tolerance, discretization, etc.) were selected after extensive tests in different examples by comparing the numerical solution and previously known results. All tests can be downloaded from Ref.[35] Also, input files used in this work are deposited in our Github repository.[36]

The WT, Delta and Omicron spike protein structures employed in our numerical calculations were obtained from a previous comprehensive simulation work on the SARS-CoV-2 variants.[21] This previous work provided atomic coordinates for six different configurations

of each variant, obtained from molecular dynamics simulations performed at 310 K in bulk water with protonation states corresponding to pH 7.4. All structures considered here correspond to the spike in its closed (down) state, which has the three RBD in the same configuration. For simplicity, we do not consider here calculations of Spike protein in the up state (with one of the three RBD in extended configuration). In the up state, the extended RBD will modify its configuration when adsorbing at a surface, so the modelling of this case will require additional simulations to determine its final configuration over the surface.

Five of these configurations (configurations labelled as 1 to 5) were identified as representative of the most populated configurations from a cluster analysis of the full MD trajectories. The clusters were created according to criteria based on the values of the Root Mean Square Deviation (RMSD) of C_α atoms and glycan carbon atoms during the MD trajectory. An additional configuration (Configuration 0) is provided as a reference structure, and it corresponds to the final configuration after the full MD trajectories. The RMSD calculated using different amino acid selections are given in the Supporting Information (Figures S2 and S3).

Models of the surfaces with uniform surface charge density appropriate for use with PyGBe were generated using a home-made python script as described in the Supporting Information.

We have considered a value of ε_r^w=80 for water and ε_r=4 for the protein and the material except otherwise indicated.

Using these models for the proteins and the surfaces, we have performed PyGBe calculations at different separations d between the protein structures and the surfaces under different conditions. We have generated input files for the following protein-surface d_c separations: 2 Å, 5Å, 10Å, 15Å, 50Å and 10^3Å (measured as the distance from the closest protein atom to the surface, see Figure 2). The largest separation is used to determine the value of the free energy at infinite protein-surface separation, G_0.

The protocol followed in our calculations was the following. In the first set of numerical calculations, we have considered all available protein structures (configurations 0 to 5) for

the three variants (WT, Delta and Omicron) in order to determine which configuration is more representative for each variant. To this end, we have considered the particular case of a strongly charged surface with $\sigma = -1$ e/nm^2 and inverse Debye length of κ=1.25 nm^{-1} (which corresponds to 150 mM of monovalent salt at 310K in water). The results for these calculations (six $\Delta G(d)$ curves for each variant) are given in the Supporting information (Figure S2). The configurations with the most favourable interactions with the surface were configuration 2 for the WT, configuration 0 for Delta and configuration 1 for Omicron.

The second set of numerical calculations was performed to obtain the three coefficients $g_{self\_prot}(d)$, $g_{\sigma}(d)$ and $g_{self\_plane}(d)$ of the free energy of interaction between each Spike variant and a charged surface (Eq.(9)) using the method developed in the previous subsection. To this end, we performed the Auxiliary I and II calculations described in Table 1 for the selected configuration of each variant. We considered κ=1.25 nm^{-1} as in the previous case. The results of the previous series of calculations were taken as the "reference system" in Table 1 (so $\sigma_{ref} = -1$ e/nm^2). The auxiliary calculations were made for all the same protein-surface separations d_c considered before and the desired coefficients $g_{self\_prot}(d_c)$, $g_{\sigma}(d_c)$, and $g_{self\_plane}(d_c)$ were computed as indicated in Table 1 (see Eqs.(10)–(12)). The obtained results for the three variants and all considered separations are compiled in Table S2 and discussed in detail in section 3.1.

In order to investigate the effect of added salt, we repeated our calculations for the case σ_{ref}=-1 e/nm^2 for each variant and three additional values of κ corresponding to monovalent salt concentrations of 15 mM, 50 mM and 1500 mM (in addition to the previous case of 150 mM). The results are reported in the next section.

Finally, in the Supporting Information, we performed an additional series of calculations to test the impact over the results of other factors (such as considering other values for the dielectric constant of the protein and testing numerical approximations).

3 Results and Discussion

3.1 Comparison between different variants (WT, Delta and Omicron) interacting with a charged surface

Let us start by comparing the interaction of the different variants of the SARS-CoV-2 spike protein (WT, Delta and Omicron) with charged surfaces in the case of κ=1.25 nm^{-1} (Debye length of $\lambda_{DH} = 1/\kappa = 0.8$ nm), which corresponds to 150 mM of monovalent salt at 310K in water.

To this end, we have computed $\Delta G(d)$ for each variant as described in section 2.4. The results are given in Table S2 and Figures 4 and 5. Overall, these results show a distinct behaviour for the Omicron variant, different from that of WT and Delta.

We first consider the results at the closest protein-surface distance ($d_c = 2$Å). As shown in Figure 4b, WT and Delta Spikes show a very similar interaction with charged surfaces, being mostly repelled by charged surfaces with little sensitivity to the sign of the surface charge. It is remarkable that in spite of its large negative charge, the WT Spike is repelled by positively charged surfaces. The only (minor) difference between WT and Delta in Figure 4b is the presence of a weak attraction between the Delta Spike and weakly charged negative surfaces (note the overall positive charge of Delta). The Omicron Spike has a completely different behaviour, being attracted by negatively charged surfaces and repelled by positively charged ones, as seen in Figure 4b. The interaction is always much stronger than the one obtained for the WT and Delta cases.

This result can be interpreted by looking at the three different terms that contribute to the free energy of interaction between each Spike variant and a charged surface (see Eq.(9)) which are shown in Figure 4c. The term g_σ, which quantifies the interaction between protein and surface charges, shows a prominent peak for the Omicron variant, being much smaller for WT and Delta (Figure 4c). The contribution of this term to ΔG (proportional to σ, see Eq.(9)) is the dominant contribution for the Omicron-surface free energy of interaction in

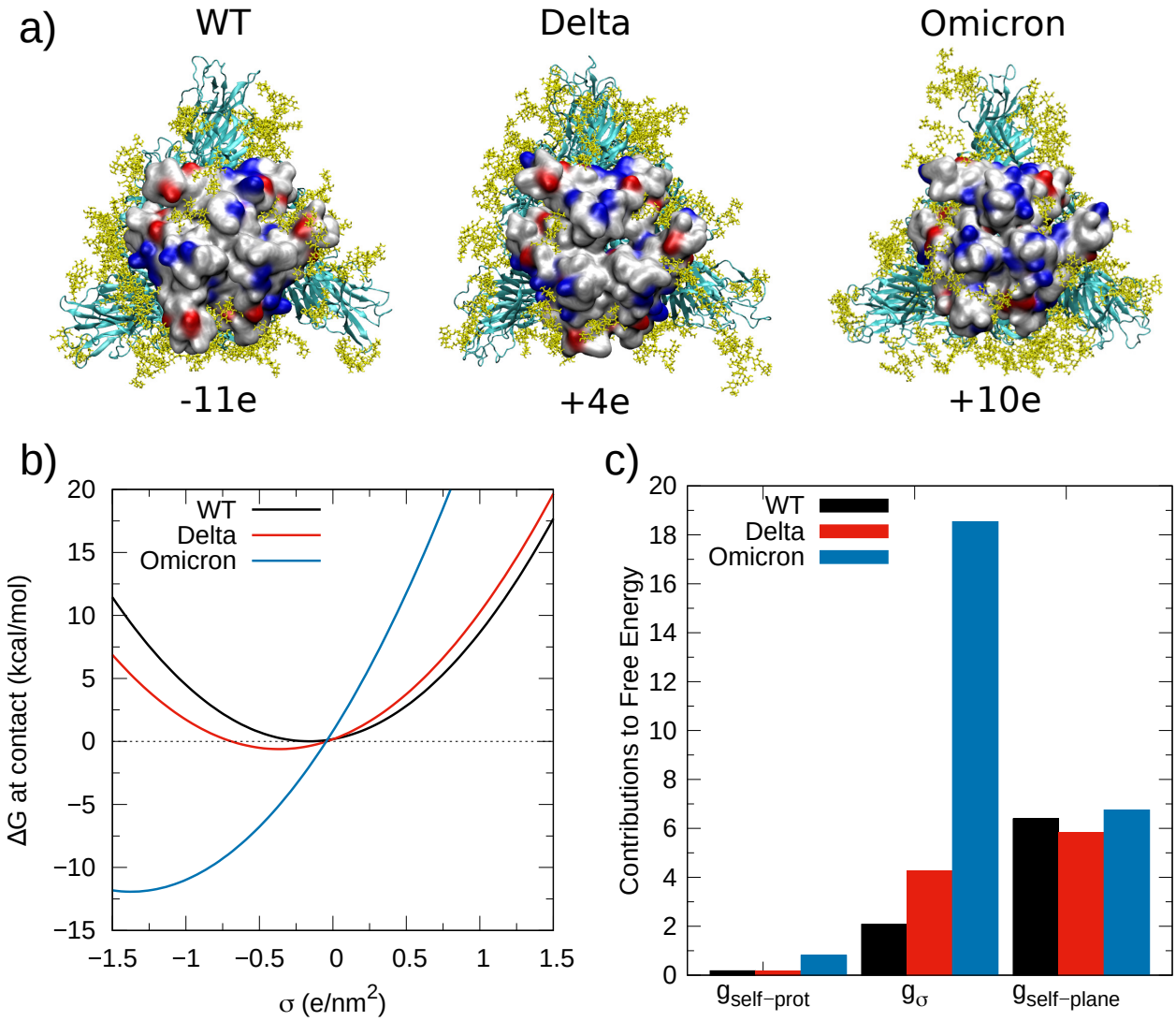

Figure 4: (a) View of the trimeric Spike protein for the WT, Delta and Omicron variants as seen from an interacting surface. The RBD domains are shown using the surface representation with basic residues in blue and acidic residues in red. Glycans are shown in yellow using bond representation. The total charge of each structure is also indicated. Images made with VMD[37]). (b) Free energy for the interaction between the different Spike protein variants and a surface with charge density σ at the distance of closest approach considered between the protein and the surface ($d_c = 2$Å), calculated using Eq. 9 (see text). (c) Histogram of the free energy contributions (Eq. 9) for each variant. Note that $g_{self\_prot}(d)$ is given in kcal/mol, $g_\sigma(d)$ in (kcal/mol)/($e\cdot$ nm^{-2}) and $g_{self\_plane}(d)$ in (kcal/mol)/($e\cdot$ nm^{-2})^2

Figure 4b. This contribution is of secondary relevance for WT and Delta (being larger for Delta than for WT).

In the case of WT and Delta, the most relevant contribution to ΔG in Figure 4b comes from the term g_{self_plane}, which encodes the repulsive interaction of the charged surface with

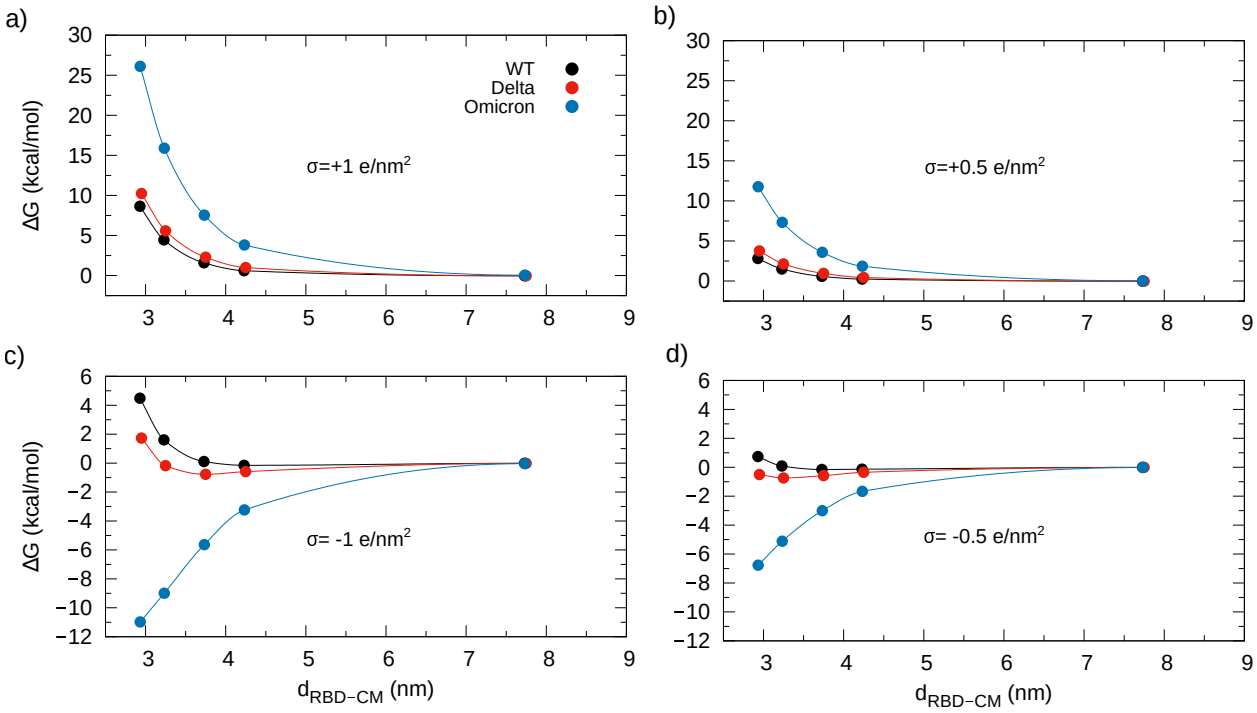

Figure 5: Free energy calculated at 5 different protein-surface separations using the coefficients given in Table S2 in Eq. 9 for the WT, Delta and Omicron variants and selected values of the surface charge σ. a) $\sigma = +1\text{e/nm}^2$, b) $\sigma = +0.5\text{e/nm}^2$, c) $\sigma = -1\text{e/nm}^2$ and d) $\sigma = -0.5\text{e/nm}^2$. Solid lines are guides to the eye.

the dielectric discontinuity at the protein/water interface. This term contributes to ΔG as $\propto \sigma^2$, and it is responsible for the shape observed for ΔG in the WT and Delta cases in Figure 4b. The value of $g_{\text{self\_plane}}$ is very similar for all three variants (Figure 4c), as expected, since it depends only on the protein size and its dielectric constant, not on the protein charge. However, this contribution is dominant for the WT and Delta variants due to the relative weakness of the direct interaction between the protein and surface charges (the g_σ term).

It should be noted that the term $g_{\text{self\_prot}}$ (due to the interaction of the protein charge with the dielectric discontinuity at the water/plane surface interface) is always very weak, with contributions of the order of the thermal energy or smaller. In general, the electrostatic interaction of all variants with neutral interfaces with dielectric discontinuities is negligible (see more details in the Supporting Information).

This different behaviour between WT and Delta from one side and Omicron on the other

side cannot be understood from its total charge. On the contrary, it reflects the distribution of charges in the Spike region exposed to the surfaces. The protein structures considered in the calculations (selected as described in section 2.4) are shown in Figure 4a, with an indication of the charged residues.

As seen in that figure, both WT and Delta Spike expose a mixture of positively and negatively charged residues towards the surface. This distribution of charges results in a weak contribution to the direct surface-protein interaction term, g_σ (Figure 4c) due to compensations between the contributions from positively and negatively charged groups. The Omicron variant is the only one that exposes a well-defined pattern of charges towards the surface, with its characteristic positively charged "bullseye" shape in its apex identified in previous works.[21] This charge distribution results in an enhanced interaction with surface charges and in a large g_σ term (Figure 4c). This feature of the charge distribution of the Omicron variant was proposed to have a decisive impact on the infection process by an enhanced electrostatic interaction with the glycocalyx.[21] Here we propose that this charge distribution is also behind the enhanced interaction with charged surfaces for the Omicron variant as found here.

The efficiency of the charge distribution of the Omicron variant to enhance the interactions with charged surfaces is in deep contrast to the inefficiency observed for the WT. Omicron and WT have total charges similar in magnitude but their distribution results in a value for the interaction term g_σ of Omicron almost 10 times larger than that for WT (see Figure 4c and Table S2). As the virus has evolved, it has not only changed from negatively to positively charged but also it changed from an inefficient to an efficient charge pattern.

This behaviour of the different contributions to the free energy for the three variants is observed not only for $d_c = 2$Å but also for all protein-surface separations considered in our calculations, as seen in Table S2. The dependence of ΔG with different protein-surface separations is computed using the coefficients in Table S2 in Eq. (9). The result is shown in Figure 5 for selected values of σ.

This figure shows again that Omicron is attracted by negatively charged surfaces and repelled by positively charged ones, with an interaction that decays monotonously with the distance (being negligible at distances much larger than the Debye length). The interaction for the WT Spike also shows a monotonous decay with the distance, being repulsive for both positively and negatively charged surfaces. The Delta variant shows a behaviour very close to that of WT for positively charged surfaces. In the case of negatively charged surfaces, it shows a slight deviation from the monotonous repulsion obtained for the WT. In this case, it is possible to see a (rather weak) attraction near the surface. In any case, the results for Delta are much closer to those obtained for WT than those obtained for Omicron.

A conclusion of this subsection is that the interaction of the Omicron spike with charged surfaces is of a different nature to that of the interaction between WT or Delta spikes with surfaces. Only the Omicron variant can be expected to be retained by charged surfaces (in fact, by negatively charged surfaces).

The results obtained in this subsection may also justify the observation made by early AFM studies that charged surfaces such as silica or glass do not substantially interact with the SARS-CoV-2 Spike protein.[14] These materials have charge densities of the order of those considered in Figure 5d.[38–40] The exact variant considered in these studies was not indicated but given the date at which these experiments were performed, it was not Omicron, which is consistent with our results. In view of our present results, it will certainly be of great interest to perform additional AFM experiments comparing the interaction of different Spike variants (WT, Delta and Omicron) with surfaces with a high negative charge such as silica. These proposed experiments will allow a direct comparison with the predictions made here of a unique behaviour for the Omicron variant.

3.2 Effect of salt concentration.

The fact that electrostatic interactions can be tuned by changing the concentration of the electrolyte could also be of interest in the case of the interaction of the SARS-CoV-2 virus

with surfaces. For example, in the coronavirus sensors in Ref.,[21] a concentration of only 10 mM of salt was considered in order to enhance electrostatic interactions. Another situation of interest is the increase in salt concentration due to evaporation. In the context of virus transmission, aerosol droplets are expelled from the respiratory system, and these droplets tend to evaporate under atmospheric conditions, causing the salt concentration to be much higher than the physiological one.[41]

Therefore, we have repeated the calculations of the previous section for different salt concentrations (15 mM, 50 mM and 1500 mM). In order to simplify the discussion, we show the results only for a highly charged negative surface ($\sigma = -1\ e/\mathrm{nm}^2$), which is the most interesting case (as seen in the previous subsection). Results for other cases can be found in the Supporting Information. The results are shown in Figure 6. We include the results of the previous subsection (corresponding to a salt concentration of 150 mM) for comparison.

The most relevant feature of the results is that in the case of the Delta variant, we obtain a significant free energy minimum (Figure 6b) at low salt concentrations (50 mM and 15 mM), which is not present at 150 mM. This means that attraction of the Delta variant by negatively charged surfaces is possible if the salt concentration is low enough. It is interesting to recall that in the case of WT, we see a similar qualitative tendency (see Figure 6a), but the attraction is too weak to be relevant. In the case of the Omicron variant, the decrease of the salt concentration increases the attraction towards negatively charged surfaces seen in the previous subsection, becoming a very strong interaction at low salt concentrations.

It is also interesting to note that most of the results discussed so far show a monotonic decay of the interaction with distance, except for a few cases with a nonmonotonic behaviour with a clear minimum (see Figure 6b,c). The reason for this nonmonotonic behaviour is the competition between an attractive and repulsive interaction with different decay lengths. Specifically, the repulsive image term, $g_{\mathrm{self\_plane}}$, with a decay length of $\lambda_D/2$, decays twice as fast as the direct interaction term, g_σ, which has a decay length of λ_D. In the case discussed in the previous subsection, this monotonic behaviour was not observable because

the repulsive interaction decays too fast ($\lambda_D/2 \sim 0.4$ nm) and the range of the repulsive interaction was not enough to produce a minimum near the surface.

In Figure 6, we also provide the results for the case of very high salt concentration (1500 mM). In that case, the electrostatic interaction is residual for all variants.

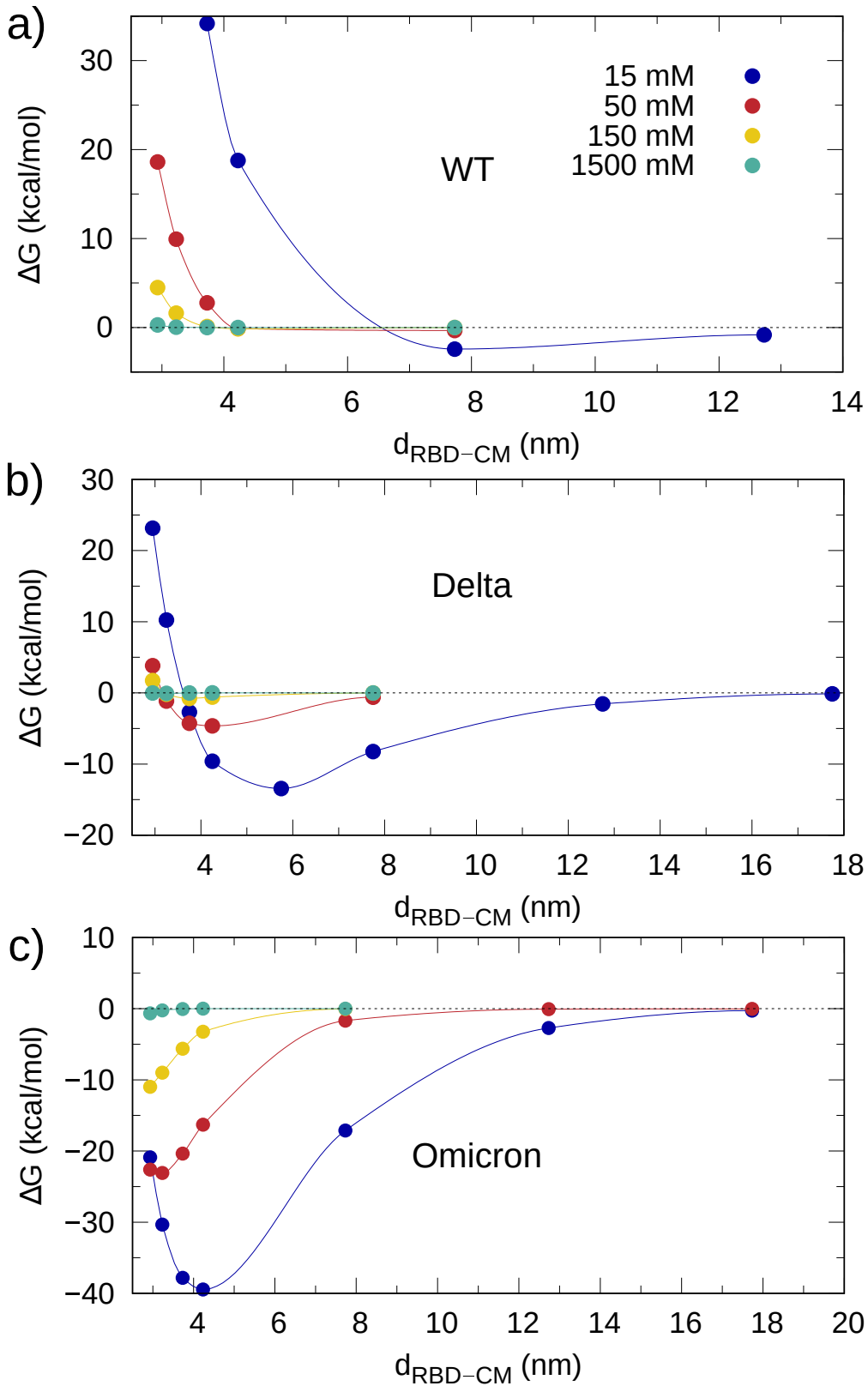

Figure 6: $\Delta G(d)$ for different salt concentrations (15 mM, 50 mM, 150 mM and 1500 mM) calculated for WT, Delta and Omicron variants and surfaces charges $\sigma = -1\ e/\mathrm{nm}^2$. (a) WT, (b) Delta and (c) Omicron. The results for 150 mM are the same as reported in section 3.1 (see Figure 5c). Solid lines are only to guide the eye.

3.3 Effect of thermal fluctuations: analysis of ΔG for different configurations of the same variant.

We argued in section 3.1 that the details of the charge distribution are very important in the interaction between the Spike protein and charged surfaces. It should be noted that the charged residues of the Spike have some flexibility and experience thermal fluctuations that may affect the details of the charge distribution close to the surface.

In order to study the possible effect of these fluctuations in the electrostatic interaction between the Spike and surfaces, we will now investigate how the obtained results depend on the particular choice of the protein configuration. To this end, we have compared the results for the six different characteristic configurations for the Spike protein identified from previous MD simulations for each variant, as described in the Methods section. We have made the comparison between the six structures of the three different variants for the particular case of $\sigma = -1\ e\cdot\ \mathrm{nm}^{-2}$ and a Debye length of $\lambda_{DH} = 1/\kappa = 0.8$ nm, as in Section 3.1. The results for all the cases are given in the Supporting Information (Figure S5). Here, we will discuss only the most relevant results.

The most interesting case corresponds to the Omicron variant, which exhibits the strongest electrostatic interactions with surfaces, as discussed in previous subsections. The results for the six available Omicron structures are summarized in Figure 7a. The interaction is always attractive, but one configuration (configuration 1) shows a significantly different free energy compared to the others, which have similar free energies (Figure 7a). Consequently, not all the configurations will be equally probable close to the surface. The protein configurations with the lowest free energy (in this case, configuration 1) will be preferentially selected. The results reported for the Omicron variant in the previous subsections correspond to configuration 1.

Let us consider the case of configurations 1 and 2 for the Omicron variant, which exhibit the most distinct interactions with the surface compared to the other configurations (see Figure 7a). ΔG at contact for configuration 1 is $\sim$1.5 times higher than that obtained

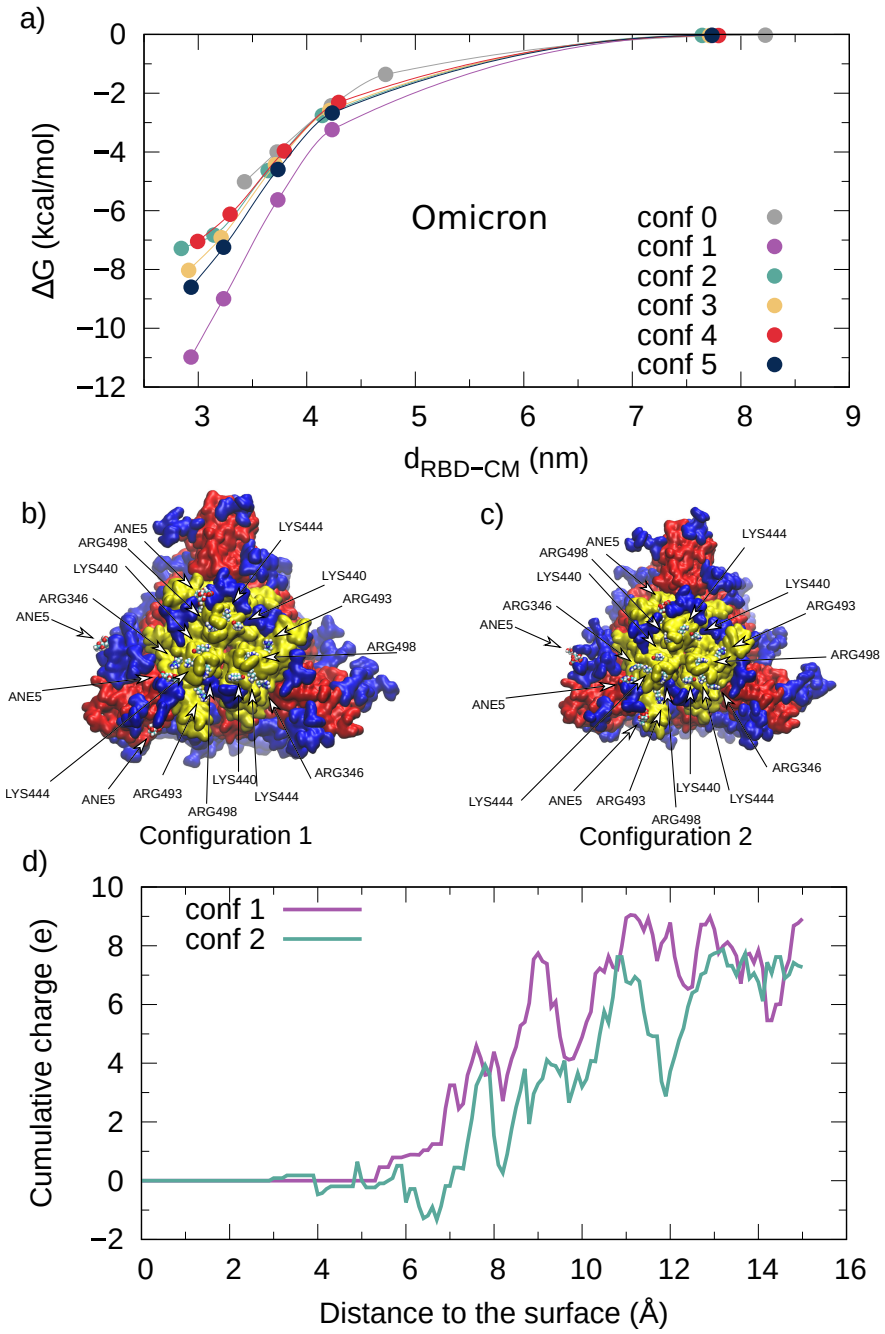

Figure 7: (a) Electrostatic free energy of the interaction between the spike protein (Omicron) and a negatively charged surface (σ=-1e · nm^{-2}). Solid lines are only to guide the eye. Bottom view of the structure of (b) configuration 1 and (c) configuration 2 of the Omicron variant, highlighting the charged residues closer to the surface. Glycans are shown in blue, the RBD in yellow (Quick Surface representation) and the rest of the protein in red. Key residues are depicted in van the der Waals representation. (d) Accumulated charge up to a given distance to the surface calculated for the configurations 1 and 2 of the Omicron variant. Spike protein images were made with VMD.[37]

for configuration 2. Snapshots of these configurations are shown in Figure 7b,c. In these snapshots, we also highlight the charged residues in the vicinity of the charged surface for these configurations. As seen in the snapshots, these structures seem almost identical, as expected from their RMSD values (see Figure S2).

However, there are small differences in the conformations of the charged residues for each configuration that affect their distances with the charged surface. The distances between the charged residues indicated in Figure 7b,c and the surface are compiled in the Supplementary Information (Table S3). This table shows that some of these charged amino acids (for example LYS440 and LYS444) are closer to the surface in configuration 1 than configuration 2. The effect of the negatively charged glycan groups are also relevant as they are closer to the surface in configuration 2 than in configuration 1 (more repulsion in configuration 2).

In order to quantify this effect of the different distances of charged residues to the surface, we have calculated the cumulative charge of the spike protein from the upper face of the planar surface ($z = 0$) to the closest region of the spike to the surface (see SI for details of the method). For the calculation, we considered the charged residues arginine, lysine, glutamate, aspartate and negatively charged glycans (ANE5). The result is shown in Figure 7d. It clearly shows that at any given distance from the surface, configuration 1 always has a higher charge than configuration 2 at close distances from the surface, justifying a stronger electrostatic attraction. This analysis shows how crucial are small differences in the position of charged amino acids.

We have also performed the same analysis for the Delta variant (Figure 8a). As in the Omicron case, there are differences between different configurations of the same Delta variant. For example, configurations 0 and 2 have a free energy minimum near the surface, whereas electrostatic interaction for configuration 4 is always repulsive. Since the interaction is rather weak, small changes in the position of charged groups have a relevant impact, changing it from weakly repulsive to weakly attractive.

We have also performed a detailed comparison between configurations 2 and 4 of the

Delta variant, as in the Omicron case. Snapshots of these structures are shown in Figures 8b and 8c. The distances between the charged residues shown in these figures and the surface are compiled in Table S4. The data shows that positively charged residues LYS444 and ARG346 are closer to the surface in configuration 2, implying a higher contribution to electrostatic attraction than in configuration 4. ASP442 is also closer in configuration 2, but the closer LYS444 residue masks this fact. There is an essential difference in the distribution of negatively charged glycans. In configuration 4, these are significantly closer than in configuration 2. It may be the cause of the electrostatic repulsion observed for configuration 4 at all separations (Figure 8a). The cumulative charge analysis shows the higher positive charge in the 17-20 Å range (Figure 8d).

It is also interesting to note that the accumulated charge for the Delta variant (Figure 8d) is substantially smaller than the accumulated charge for the Omicron variant (Figure 7d), justifying the much stronger interaction found in the later case.

The results for the WT show a similar behaviour, as shown in the Supporting Information (Figure S5). The interaction between the spike protein and the surface is repulsive for all the configurations considered of the WT protein.

In summary, we have found that for WT, Delta and Omicron variants, significant differences in ΔG are observed for different configurations within the same variant. This result highlights the importance of taking into account the detailed charge distribution (which may change over time due to the change in relative positions of labile amino acids) instead of considering only the total charge.

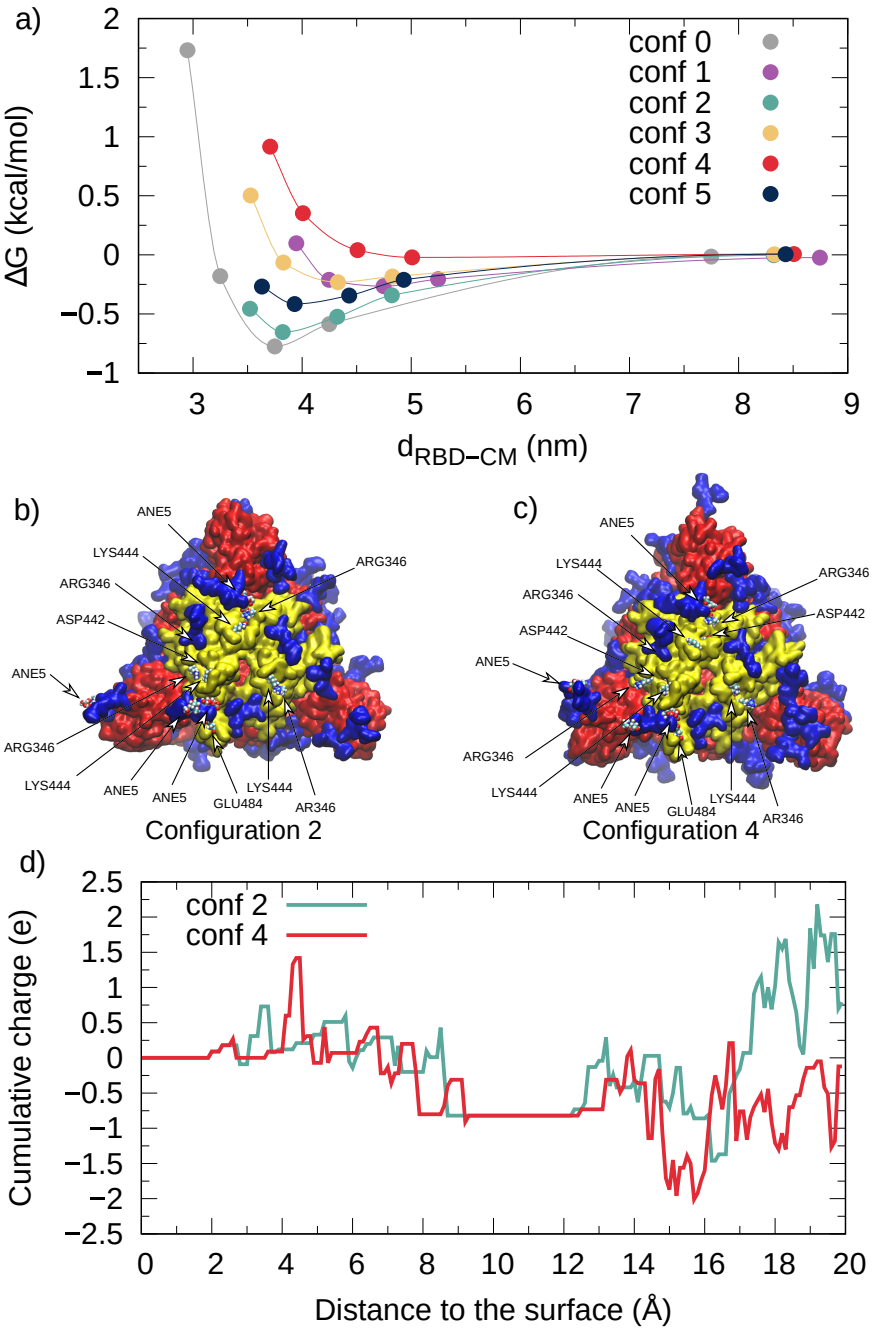

Figure 8: (a) Electrostatic free energy of the interaction between the spike protein (Delta variant) and a negatively charged surface (σ=-1e · nm^{-2}). Solid lines are only to guide the eye. Bottom view of the structure of configuration 2 (b) and configuration 4 (c) of the Delta variant, highlighting the charged residues closer to the surface. Glycans are shown in blue, the RBD in yellow (Quick Surface representation) and the rest of the protein in red. Key residues are depicted in Van der Waals representation. (d) Accumulated charge up to a given distance to the surface calculated for the configurations 2 and 4 of the Omicron variant. Spike protein images were made with VMD.[37]

4 Conclusions

Arguably, one of the most important changes observed in the SARS-CoV-2 evolved variants was the change in the electrostatic charge of its Spike protein. It evolved across the variants from the highly negative Wild Type (WT) to the highly positive Omicron variant. Even more importantly, the charge distribution of the receptor binding domain of the Spike protein evolved from a mixed distribution of positively and negatively charged residues in WT and Delta to a pattern with highly localized positively charged residues in Omicron. This evolution has a decisive impact on virus-cell interactions key to the infection process, as demonstrated in previous studies.[19,21,22]

Our results show that this evolution has also a decisive impact on the mechanism of interaction of the SARS-CoV-2 virus with charged surfaces. The interaction of the WT and Delta variant spikes with charged surfaces is dominated by repulsive image forces (proportional to σ^2) which are generated at the protein/water interface. The Omicron variant shows a distinct behaviour, being strongly attracted to negatively charged surfaces and repelled from positively charged ones. Therefore, the virus has evolved from being repelled by charged surfaces to efficiently adsorbing to negatively charged ones.

The fact that the Omicron variant has a more homogeneous, well-defined charge distribution substantially enhances its electrostatic interactions. Omicron exposes positively charged residues and consequently is attracted by negatively charged surfaces and repelled by positively charged ones. On the contrary, the heterogeneous charge distribution in the Wild Type and Delta spike proteins produces an inefficient (weak) direct electrostatic interaction with charged surfaces. In these circumstances, the image charge repulsion originated at the protein/water dielectric discontinuity dominates the interaction. We therefore conclude that the interaction of Omicron with surfaces is of a different nature than that of WT and Delta.

Our results also imply that only the Omicron variant can be expected to be retained by charged surfaces (in fact, by negatively charged surfaces). Since many commonly charged surfaces are negatively charged (such as silicate glass, silica and common textiles), this result

has important implications for situations involving interactions of the SARS-CoV-2 virus and materials. For example, electrostatic retention of viruses by filters made of charged fibers can be expected to be relevant for the Omicron variant but not for the original WT virus or the Delta variant. Also, contamination of negatively charged surfaces by SARS-CoV-2 viruses (fomites) can only be expected to occur with the Omicron variant but not with the original WT. It is also interesting to note that the most effective coatings against the formation of bacterial biofilms (preventing bacterial adhesion) are negatively charged.[42] These materials may also prevent the adhesion of WT and Delta variants of SARS-CoV-2 viruses, but they will promote the adhesion of Omicron.

Finally, we would like to emphasize that the calculations made here were performed using a new method (based on Debye-Hückel theory) that provides efficient and generalized results as a function of the surface charge density σ. The method provides a general analytical expression for the free energy of interaction between an atomistic model of a protein and a surface with arbitrary surface charge σ. The method is based on an exact expression for the free energy in terms of three different contributions: the interaction (independent of σ) of the charged protein with the surface/water dielectric discontinuity, the interaction (proportional to σ^2) of the surface charge with the protein/water dielectric discontinuity and the direct protein-surface interactions proportional to σ. These three terms are efficiently determined by employing a set of three appropriately designed numerical calculations independent of σ. The applicability of the method is not limited to the specific case studied here but to any other problems involving the interaction of a protein with a charged surface within the scope of the linear Poisson-Boltzmann equation. This approach, coupled with numerical PB solvers, offers a powerful tool for systematically studying protein-surface interactions with charged surfaces.

Acknowledgement

This work was supported by Grant No. PID2021-124297NB-C33 funded by MICIU/AEI/10.13039/501100011033, the "Severo Ochoa" Grant No. CEX2023-001263-S for Centers of Excellence awarded to ICMAB, and the FPI under Grant No. PRE2020-093689 awarded to M.D. We also thank the Government of Catalonia (AGAUR) under Grant No. 2021SGR01519. H.V.G. acknowledges financial support from the Maria Zambrano Grant No. CA6/RSUE/2022-00108 and Ramon y Cajal grant No. RYC2022-038082-I. M.K. acknowledges financial support from the Slovenian Research and Innovation Agency ARIS (contracts P1-0055 and J1-4382). We thank the CESGA supercomputing center for computer time and technical support at the Finisterrae supercomputer. We thank Dr. Fiona L. Kearns (UCSD) for discussions regarding the spike protein structures.

M.D. is enrolled in the Material Sciences Ph.D. program of the Universitat Autònoma de Barcelona.

Supporting Information Available

Methodology details and Additional results.

References

(1) Gerba, C. P. In *Advances in Applied Microbiology*; Laskin, A. I., Ed.; Academic Press, 1984; Vol. 30; pp 133–168.

(2) Armanious, A.; Aeppli, M.; Jacak, R.; Refardt, D.; Sigstam, T.; Kohn, T.; Sander, M. Viruses at Solid–Water Interfaces: A Systematic Assessment of Interactions Driving Adsorption. *Environmental Science & Technology* **2016**, *50*, 732–743, Publisher: American Chemical Society.

(3) Gentile, G. J.; Cruz, M. C.; Rajal, V. B.; Fidalgo de Cortalezzi, M. M. Electrostatic interactions in virus removal by ultrafiltration membranes. *Journal of Environmental Chemical Engineering* **2018**, *6*, 1314–1321.

(4) Chattopadhyay, S.; Puls, R. W. Forces dictating colloidal interactions between viruses and soil. *Chemosphere* **2000**, *41*, 1279–1286.

(5) Zhang, D.; Li, Q.; Prigiobbe, V. Population balance modeling of homogeneous viral aggregation. *Chemical Engineering Science* **2022**, *247*, 117035.

(6) Hernando-Pérez, M.; Cartagena-Rivera, A. X.; Božič, A. L.; Carrillo, P. J. P.; Martín, C. S.; Mateu, M. G.; Raman, A.; Podgornik, R.; Pablo, P. J. d. Quantitative nanoscale electrostatics of viruses. *Nanoscale* **2015**, *7*, 17289–17298, Publisher: The Royal Society of Chemistry.

(7) Cooper, C. D.; Addison-Smith, I.; Guzman, H. V. Quantitative electrostatic force tomography for virus capsids in interaction with an approaching nanoscale probe. *Nanoscale* **2022**, *14*, 12232–12237.

(8) D. Cooper, C.; C. Clementi, N.; Forsyth, G.; A. Barba, L. PyGBe: Python, GPUs and Boundary elements for biomolecular electrostatics. *The Journal of Open Source Software* **2016**, *1*, 43.

(9) Addison-Smith, I.; Guzman, H. V.; Cooper, C. D. Accurate Boundary Integral Formulations for the Calculation of Electrostatic Forces with an Implicit-Solvent Model. *Journal of Chemical Theory and Computation* **2023**, *19*, 2996–3006, Publisher: American Chemical Society.

(10) Dimitrov, D. S. Virus entry: molecular mechanisms and biomedical applications. *Nature Reviews Microbiology* **2004**, *2*, 109–122, Publisher: Nature Publishing Group.

(11) Sikora, M.; Bülow, S. v.; Blanc, F. E. C.; Gecht, M.; Covino, R.; Hummer, G. Computational epitope map of SARS-CoV-2 spike protein. *PLOS Computational Biology* **2021**, *17*, e1008790, Publisher: Public Library of Science.

(12) Joonaki, E.; Hassanpouryouzband, A.; Heldt, C. L.; Areo, O. Surface Chemistry Can Unlock Drivers of Surface Stability of SARS-CoV-2 in a Variety of Environmental Conditions. *Chem* **2020**, *6*, 2135–2146.

(13) Bosch, A. M.; Guzman, H. V.; Pérez, R. Adsorption-Driven Deformation and Footprints of the RBD Proteins in SARS-CoV-2 Variants on Biological and Inanimate Surfaces. *Journal of Chemical Information and Modeling* **2024**, *64*, 5977–5990, Publisher: American Chemical Society.

(14) Xie, L.; Liu, F.; Liu, J.; Zeng, H. A Nanomechanical Study on Deciphering the Stickiness of SARS-CoV-2 on Inanimate Surfaces. *ACS Applied Materials & Interfaces* **2020**, *12*, 58360–58368.

(15) Xiao, Y.; Zheng, B.; Ding, X.; Zheng, P. Probing nanomechanical interactions of SARS-CoV-2 variants Omicron and XBB with common surfaces. *Chemical Communications* **2023**, *59*, 11268–11271.

(16) Adamczyk, Z.; Batys, P.; Barbasz, J. SARS-CoV-2 virion physicochemical characteristics pertinent to abiotic substrate attachment. *Current Opinion in Colloid & Interface Science* **2021**, *55*, 101466.

(17) Mateos, H.; Mallardi, A.; Camero, M.; Lanave, G.; Catella, C.; Buonavoglia, A.; De Giglio, O.; Buonavoglia, C.; Palazzo, G. Mechanism of surfactant interactions with feline coronavirus: A physical chemistry perspective. *Journal of Colloid and Interface Science* **2024**, *662*, 535–544.

(18) Domingo, M.; Faraudo, J. Effect of surfactants on SARS-CoV-2: Molecular dynamics simulations. *The Journal of Chemical Physics* **2023**, *158*, 114107.

(19) Sang, P.; Chen, Y.-Q.; Liu, M.-T.; Wang, Y.-T.; Yue, T.; Li, Y.; Yin, Y.-R.; Yang, L.-Q. Electrostatic Interactions Are the Primary Determinant of the Binding Affinity of SARS-CoV-2 Spike RBD to ACE2: A Computational Case Study of Omicron Variants. *International Journal of Molecular Sciences* **2022**, *23*, 14796, Number: 23 Publisher: Multidisciplinary Digital Publishing Institute.

(20) Božič, A.; Podgornik, R. Evolutionary changes in the number of dissociable amino acids on spike proteins and nucleoproteins of SARS-CoV-2 variants. *Virus Evolution* **2023**, *9*, vead040.

(21) Kim, S. H.; Kearns, F. L.; Rosenfeld, M. A.; Votapka, L.; Casalino, L.; Papanikolas, M.; Amaro, R. E.; Freeman, R. SARS-CoV-2 evolved variants optimize binding to cellular glycocalyx. *Cell Reports Physical Science* **2023**, *4*, 101346.

(22) Kearns, F. L.; Sandoval, D. R.; Casalino, L.; Clausen, T. M.; Rosenfeld, M. A.; Spliid, C. B.; Amaro, R. E.; Esko, J. D. Spike-heparan sulfate interactions in SARS-CoV-2 infection. *Current Opinion in Structural Biology* **2022**, *76*, 102439.

(23) Javidpour, L.; Božič, A.; Naji, A.; Podgornik, R. Electrostatic interactions between the SARS-CoV-2 virus and a charged electret fibre. *Soft Matter* **2021**, *17*, 4296–4303.

(24) Moreira, R. A.; Guzman, H. V.; Boopathi, S.; Baker, J. L.; Poma, A. B. Characterization of Structural and Energetic Differences between Conformations of the SARS-CoV-2 Spike Protein. *Materials* **2020**, *13*, 5362, Number: 23 Publisher: Multidisciplinary Digital Publishing Institute.

(25) Malaspina, D. C.; Faraudo, J. Computer simulations of the interaction between SARS-CoV-2 spike glycoprotein and different surfaces. *Biointerphases* **2020**, *15*, 051008.

(26) Domingo, M.; Faraudo, J. Interaction between SARS-CoV-2 spike glycoprotein and human skin models: a molecular dynamics study. *Soft Matter* **2021**, *17*, 9457–9468.

(27) Sahihi, M.; Faraudo, J. Computer Simulation of the Interaction between SARS-CoV-2 Spike Protein and the Surface of Coinage Metals. *Langmuir* **2022**, *38*, 14673–14685.

(28) Sahihi, M.; Faraudo, J. Molecular Dynamics Simulations of Adsorption of SARS-CoV-2 Spike Protein on Polystyrene Surface. *Journal of Chemical Information and Modeling* **2022**, *62*, 3814–3824.

(29) Verwey, E. J. W. E. J. W.; Overbeek, J. T. G.; Nes, K. v. *Theory of the stability of lyophobic colloids / E.J.W. Verwey and J. Th. G. Overbeek ; with the collaboration of K. van Nes*; Dover: Mineola (N.Y.), 1999; Publication Title: Theory of the stability of lyophobic colloids.

(30) Cooper, C. D.; Bardhan, J. P.; Barba, L. A biomolecular electrostatics solver using Python, GPUs and boundary elements that can handle solvent-filled cavities and Stern layers. *Computer Physics Communications* **2014**, *185*, 720–729.

(31) Cooper, C. D.; Clementi, N. C.; Barba, L. A. Probing protein orientation near charged nanosurfaces for simulation-assisted biosensor design. *The Journal of Chemical Physics* **2015**, *143*, 124709.

(32) Urzúa, S. A.; Sauceda-Oloño, P. Y.; García, C. D.; Cooper, C. D. Predicting the Orientation of Adsorbed Proteins Steered with Electric Fields Using a Simple Electrostatic Model. *The Journal of Physical Chemistry B* **2022**, *126*, 5231–5240.

(33) Martínez, M.; Cooper, C. D.; Poma, A. B.; Guzman, H. V. Free Energies of the Disassembly of Viral Capsids from a Multiscale Molecular Simulation Approach. *Journal of Chemical Information and Modeling* **2020**, *60*, 974–981.

(34) Kanduč, M.; Naji, A.; Forsman, J.; Podgornik, R. Dressed counterions: Strong electrostatic coupling in the presence of salt. *The Journal of Chemical Physics* **2010**, *132*, 124701.

(35) Domingo, M. Github repository tutorial. `https://github.com/soft-matter-theory-at-icmab-csic/pygbe_tutorial`.

(36) Domingo, M. GitHub repository input files. `https://github.com/soft-matter-theory-at-icmab-csic/spike_surface_electrostatics`.

(37) Humphrey, W.; Dalke, A.; Schulten, K. VMD: Visual molecular dynamics. *Journal of Molecular Graphics* **1996**, *14*, 33–38.

(38) Behrens, S. H.; Grier, D. G. The charge of glass and silica surfaces. *The Journal of Chemical Physics* **2001**, *115*, 6716–6721.

(39) Emami, F. S.; Puddu, V.; Berry, R. J.; Varshney, V.; Patwardhan, S. V.; Perry, C. C.; Heinz, H. Force Field and a Surface Model Database for Silica to Simulate Interfacial Properties in Atomic Resolution. *Chemistry of Materials* **2014**, *26*, 2647–2658.

(40) Choi, Y. K.; Kern, N. R.; Kim, S.; Kanhaiya, K.; Afshar, Y.; Jeon, S. H.; Jo, S.; Brooks, B. R.; Lee, J.; Tadmor, E. B.; Heinz, H.; Im, W. CHARMM-GUI Nanomaterial Modeler for Modeling and Simulation of Nanomaterial Systems. *Journal of Chemical Theory and Computation* **2022**, *18*, 479–493.

(41) Poon, W. C. K.; Brown, A. T.; Direito, S. O. L.; Hodgson, D. J. M.; Le Nagard, L.; Lips, A.; MacPhee, C. E.; Marenduzzo, D.; Royer, J. R.; Silva, A. F.; Thijssen, J. H. J.; Titmuss, S. Soft matter science and the COVID-19 pandemic. *Soft Matter* **2020**, *16*, 8310–8324.

(42) Rzhepishevska, O.; Hakobyan, S.; Ruhal, R.; Gautrot, J.; Barbero, D.; Ramstedt, M. The surface charge of anti-bacterial coatings alters motility and biofilm architecture. *Biomaterials Science* **2013**, *1*, 589–602, Publisher: Royal Society of Chemistry.

TOC Graphic